Available online at www.sciencedirect.com
ScienceDirect
International Journal of Heat and Mass Transfer 51 (2008) 977–992
International Journal of HEAT and MASS TRANSFER
www.elsevier.com/locate/ijhmt

Distribution of air–water annular flow in a header of a parallel flow heat exchanger

Nae-Hyun Kim *, Sung-Pil Han

Department of Mechanical Engineering, University of Incheon, 177 Dohwa-Dong, Nam-Gu, Incheon 402-749, Republic of Korea

Received 22 November 2006; received in revised form 4 April 2007
Available online 20 August 2007

Abstract

The air and water flow distribution are experimentally studied for a heat exchanger composed of round headers and 10 flat tubes. The effects of tube protrusion depth as well as header mass flux, and quality are investigated, and the results are compared with previous 30 channel data. The flow at the header inlet is annular. For the downward flow configuration, water flow distribution is significantly affected by tube protrusion depth. For flush-mounted geometry, significant portion of water flows through frontal part of the header. As the protrusion depth increases, more water is forced to rear part of the header. The effect of header mass flux or quality is qualitatively the same as that of the protrusion depth. For the upward flow configuration, however, significant portion of water flows through rear part of the header. The effect of protrusion depth is the same as that of the downward flow. However, the effect of header mass flux or quality is opposite to the downward flow case. Compared with the previous 30 channel configuration, the present 10 channel configuration yields better flow distribution. Possible explanation is provided from flow visualization results.

Keywords: Flow distribution; Parallel flow heat exchanger; Air–water flow; Header; Annular flow

1. Introduction

Brazed aluminium heat exchangers consist of flat tubes of 1–2 mm hydraulic diameter on the refrigerant-side, and louver fins on the air-side. They are seriously considered as evaporators of residential air conditioners due to the superior thermal performance as compared with conventional fin-tube heat exchangers. For a brazed aluminium heat exchanger, a number of tubes are grouped to one pass using a header to manage the excessive tube-side pressure drop by small channel size. To use the brazed aluminium heat exchanger as a refrigerant evaporator, it is very important to evenly distribute the two-phase refrigerant (especially the liquid) into each tube. Otherwise, the thermal performance is significantly deteriorated. According to Kulkarni et al. [1], the performance reduction by flow mal-distribution could be as large as 20%. For an evaporator usage, the flat tubes are installed vertically (with headers in horizontal position) to facilitate the air-side condensate drainage. The number of flat tubes could be as much as several hundreds depending on thermal loads. In such a case, the refrigerant-side is circuited to a multi-pass to maintain acceptable refrigerant velocity and to improve the refrigerant distribution. In an evaporator, the number of tubes per pass increases in a flow direction to accommodate the increased refrigerant velocity. For a condenser, on the contrary, the number of tubes per pass decreases in a flow direction. The number of tubes per pass (or the header length per pass) will significantly influence the flow distribution. In addition to the header length, the flow direction, the tube protrusion depth into the header as well as the flow velocity and the quality will also affect the flow distribution. Webb and Chung [2], Hrnjak [3], Lee [4] provide recent reviews on this subject.

The literature reveals several studies on the two-phase distribution in a header – branch tube configuration. Watanabe et al. [5] conducted a flow distribution study

* Corresponding author. Tel.: +82 32 770 8420; fax: +82 32 770 8410.
E-mail address: knh0001@incheon.ac.kr (N.-H. Kim).

0017-9310/$ - see front matter © 2007 Elsevier Ltd. All rights reserved.
doi:10.1016/j.ijheatmasstransfer.2007.05.028

Nomenclature

D	header inner diameter (m)	h	protrusion depth (m)
Fr	Froude number (Eq. (1))	SD	standard deviation
G	mass flux in a header (kg/m^2 s)	x	vapour quality in a header
g	gravitational constant (m s^{-2})	ρ_l	liquid density (kg m^{-3})
G_{eff}	effective header mass flux based on the flow area seen by the flow (kg/m^2 s)	ρ_v	vapour density (kg m^{-3})

for a round header (20 mm ID) – four round tube (6 mm ID) upward flow configuration using R-11. The mass flux (based on the header cross-sectional area) was varied from 40 to 120 kg/m^2 s, and the inlet quality was varied up to 0.4. The flow in the header inlet was mostly stratified. The flow distribution was highly dependent on the mass flux and the quality. Tompkins et al. [6] tested a rectangular header – 15 flat tube downward flow configuration using air–water. The header mass flux was varied from 50 to 400 kg/m^2 s, and the quality was varied up to 0.4. The flow in the header inlet was stratified at low mass fluxes, and it was annular at high mass fluxes. The flow distribution was highly dependent on the mass flux and the quality. Better distribution was obtained at a lower mass flux (stratified flow regime). Vist and Pettersen [7] investigated a round header (8 mm and 16 mm ID) – 10 round tube (4 mm ID) configuration using R-134a. Both upward and downward flow were tested. The mass flux (based on the branch tube) was varied from 124 to 836 kg/m^2 s, and the quality was varied up to 0.5. The flow in the header inlet was mostly intermittent with some annular at high mass fluxes. For the downward flow configuration, most of the liquid flowed through frontal part of the header. For the upward configuration, on the contrary, most of the liquid flowed through the rear part of the header. The liquid distribution improved as the vapour quality decreased. The mass flux had negligible effect on the flow distribution. Lee and Lee [8] investigated the effect of the tube protrusion depth for a vertical rectangular header (24 by 24 mm) – five horizontal rectangular branch tube configuration using air–water. The flow in the header inlet was annular. The flow distribution was highly dependent on the protrusion depth. As the protrusion depth increased, more water flowed through the downstream part of the header. Cho et al. [9] investigated the effect of the header orientation (vertical and horizontal) and the refrigerant inlet pipe direction (inline, cross, parallel) for a round header – 15 flat tube configuration using R-22. The header mass flux was fixed at 60 kg/m^2 s, and the quality was varied up to 0.3. For the vertical header configuration, most of the liquid flowed through the frontal part of the header, and the effect of the inlet pipe direction was not significant. For a horizontal header, the flow distribution was highly dependent on the inlet pipe direction, and better distribution was obtained for the parallel or the cross flow configuration. Koyama et al. [10] investigated the effect of varying the tube protrusion depth for a horizontal round header (9 mm ID) and six vertical flat tube configuration using R-134a. The header mass flux was fixed at 130 kg/m^2 s, and the quality was varied up to 0.4. Tests were conducted for the downward configuration, and the flow at the header inlet was identified as intermittent. The protrusion depth was systematically varied, and the optimum configuration was found to be with front two tubes protruded to the center of the header and the remaining four tubes flush-mounted. Better liquid distribution was obtained at a lower vapour quality. Bowers et al. [11] investigated the effect of tube protrusion depth as well as the effect of the entrance length for a downward configuration using R-134a. Their test section composed of horizontal round header (20 mm ID) and 15 vertical flat tubes. The header mass flux was varied from 46 to 107 kg/m^2 s, and the quality was varied up to 0.35. The apparatus was equipped an expansion valve, and expanded two-phase mixture was supplied to the test section through the entrance tube. For a short entrance length of 89 mm, the liquid distribution was relatively uniform with minor influence of protrusion depth, mass flux or quality. For a long entrance length of 267 mm, however, better distribution was obtained as the mass flux or the protrusion depth increased. Kim and Sin [12] also investigated the effect of tube protrusion depth for a round header (17 mm ID) and 30 flat tube ($D_h = 1.32$ mm) configuration using air and water. Both upward and downward configuration was tested. The header mass flux was varied from 70 to 130 kg/m^2 s, and the quality was varied up to 0.6. The flow at the header inlet was annular. For the downward flow configuration, most of the water flowed through frontal part of the header, and the effect of tube protrusion depth, mass flux or quality was significant. As the protrusion depth, mass flux or quality increased, more water was forced to rear part of the header. For upward flow configuration, however, most of the water flowed through rear part of the header, and the effect of the above mentioned parameters was insignificant. Rong et al. [13], Bernoux et al. [14] provide flow distribution data for a plate heat exchanger geometry.

The above literature survey reveals that the two-phase flow distribution in a header – branch tube configuration is very complex. Many parameters, both geometric and flow, affect the results, and more data are needed on this subject. Especially, the effect of number of tubes (or header

length) has not been investigated yet. This study is a continuing effort succeeding Kim and Sin [12], who investigated the air–water flow distribution in a parallel flow heat exchanger comprised round header and 30 branch flat tubes. In this study, the same header (ID = 17 mm), and flat tube ($D_h = 1.32$ mm) configuration was tested. However, the number of tube was reduced to 10. The header mass flux and the quality were varied for $70 \leqslant G \leqslant 130\ \mathrm{kg/m^2\,s}$ and $0.2 \leqslant x \leqslant 0.6$. The effects of the flow direction (upward or downward) and the tube protrusion depth (non-dimensional protrusion depth, $h/D = 0.0, 0.25, 0.5$) were also investigated, and the results are compared with the 30 channel data of Kim and Sin [12]. One thing to note is that the practical protrusion depth of the brazed aluminium heat exchanger having 17 mm ID header and 16 mm width flat tube is $h/D = 0.5$ to avoid clogging with brazing flux.

2. Experimental apparatus

A schematic drawing of the experimental apparatus is shown in Fig. 1. The test section consists of the 17 mm ID upper and lower headers, which are 91 cm apart, and branch flat tubes inserted at 9.8 mm pitches. This configuration was chosen to simulate the actual parallel flow heat exchanger. The cross-section of the present flat tube is shown in Fig. 2. The tube is made by extrusion from an aluminium stock. In Fig. 2, the tube wall is hatched to distinguish it from the flow channel. The hydraulic diameter is 1.32 mm, and the flow cross-sectional area is 12.24 $\mathrm{mm^2}$. The headers were made of transparent PVC for flow visualization. A 17 mm hole was machined longitudinally in a square PVC rod (25 mm × 25 mm × 400 mm), and 10 flat holes for insertion of flat tubes were machined at the bottom. An aluminium plate, which had matching flat holes, was installed underneath the header as illustrated in Fig. 3. Flat tubes were secured, and the protrusion depth was adjusted using O-rings between the header and the aluminium plate. Transition blocks were installed in the test section to connect the flat tubes and the 6.0 mm ID round tubes. The round tubes served as flow measurement lines. At the inlet of the header, 1.0 m long copper tube having the same inner diameter as the header was attached. The tube served as the flow development section.

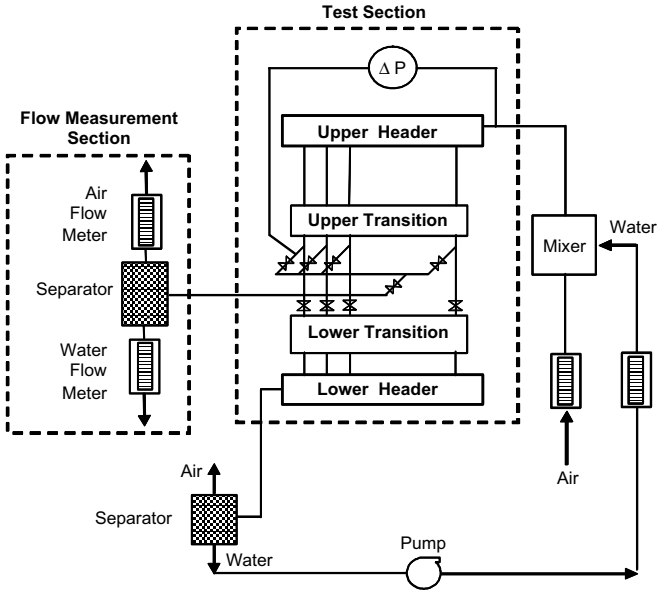

Fig. 1. Schematic drawing of the apparatus.

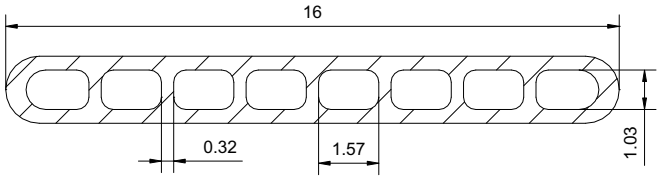

Fig. 2. Cross-sectional view of the flat tube used in this study (unit: mm).

The water and air, whose flow rates are separately determined, are mixed in a mixer before the air–water mixture is introduced into the header. The flow rate of every other flat tube is measured by directing the air–water mixture to the separator in the flow measurement section. As shown in Fig. 1, two valves – one at the main stream, the other at the bypass stream – are installed at every other channel. Normally, main stream valves are open, and bypass stream valves are closed. To measure the flow rate at a certain channel, the main stream valve is closed, and the bypass valve is open. The flow measurement principle is illustrated in Fig. 4. To prevent possible flow pattern change before and during the measurement, the differential pressure between the inlet of the upper header and the transition section was maintained the same by controlling the valve in the transition section. The pressure fluctuations during measurement were within 10% of the average value. The total water and air flow rates to the header were measured by a mass flow meter (accuracy: 1.5×10^{-6} kg/s) and a float type flow meter (accuracy: 1%), respectively. The air flow rate out of the separator was measured by a float type flow meter (accuracy: 1%), and the water flow rate out of the separator was measured by weighing the drained water in a graduated cylinder. During the whole series of tests, several runs were made to check the repeatability of the data. The data were repeatable within 10%. The maximum experimental uncertainty was 10% for the water flow rate measurement, and 5% for the air flow rate measurement. When the channel water or air flow rates were added and compared with the supplied water or air flow rates (for the channels where flow rates were not measured, the average values of the upstream and downstream channel flow rates were used), they agreed within 10%.

Tests were conducted with the inlet and the exit located at the same side of the test section (reverse configuration). The inlet and the exit may be located at the opposite side of the test section (parallel configuration). Kim and Sin [12] have shown that the water flow distribution is negligibly different between the reverse and the parallel configuration. For a single phase flow, however, different flow distribution between the reverse and the parallel configuration was

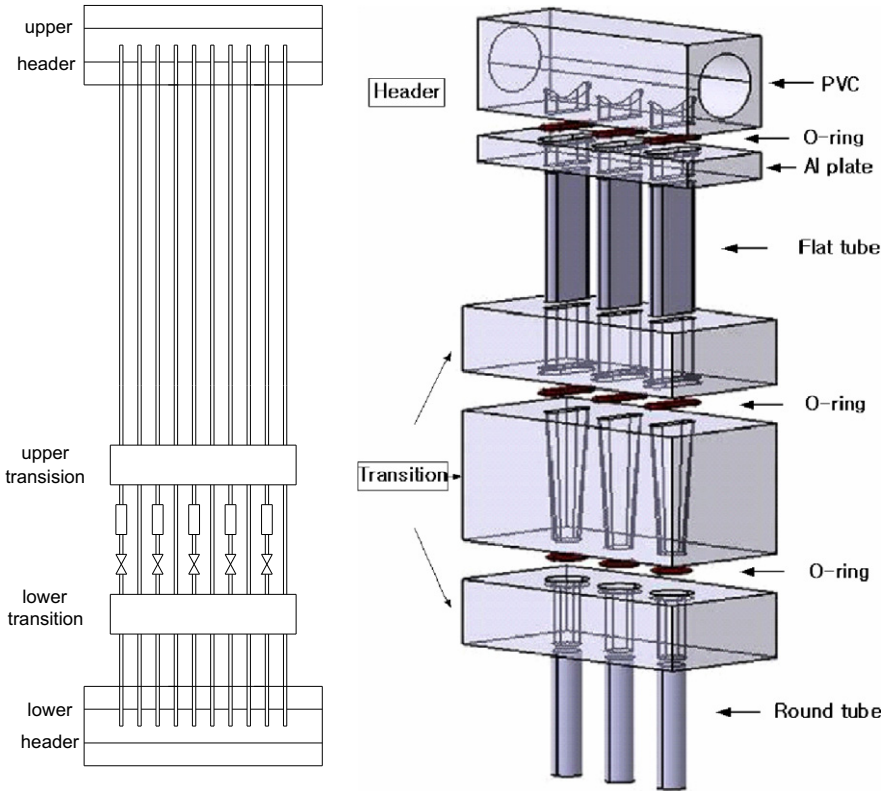

Fig. 3. Detailed drawing of the test section.

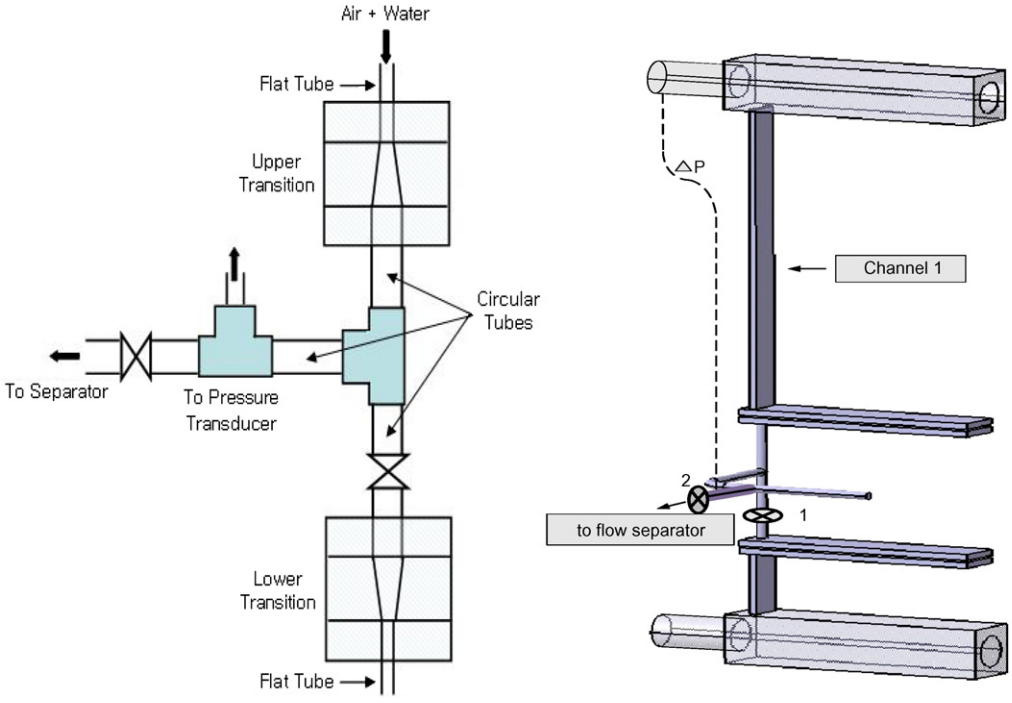

Fig. 4. Schematic drawing illustrating the flow measurement method.

reported by Bajura and Jones [15] and Yin et al. [16]. As shown by Bajura and Jones [15], the pressure difference between the upper and lower header determines the flow distribution. The pressure drop in the header is the sum of the friction and the acceleration components. In the upper header, the flow is decelerated due to the loss of flow to branch tubes. This results in a pressure rise, which acts counter to the friction term. However, in the bottom

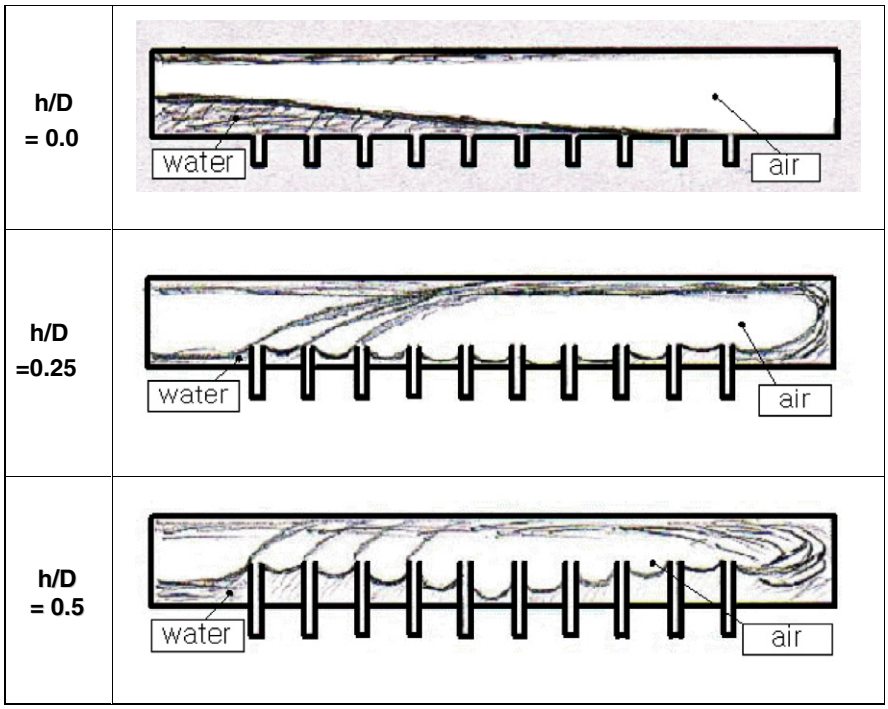

(a) Typical flow pattern in a 10 channel header with downward configuration

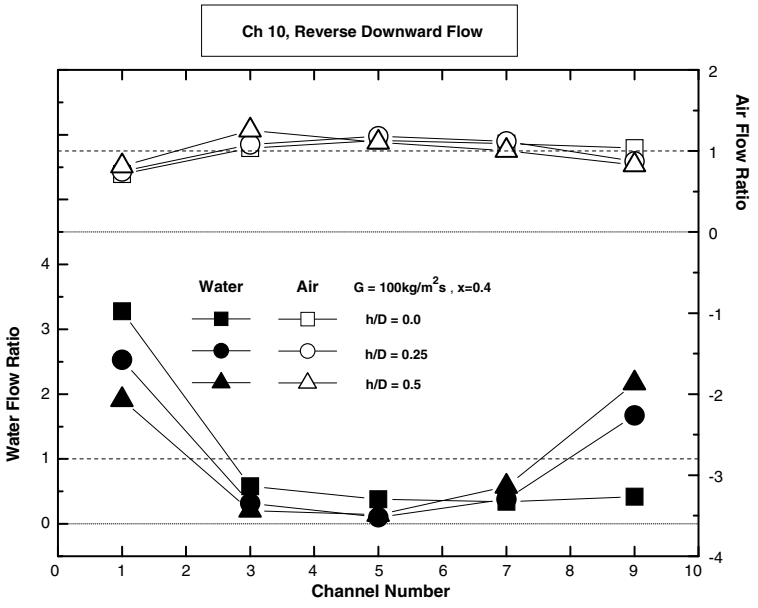

(b) Corresponding water and air distribution

Fig. 5. Typical flow pattern in a upper 10 channel header with downward flow configuration and the corresponding water and air distribution: (a) typical flow pattern in a 10 channel header with downward configuration and (b) corresponding water and air distribution.

header, the flow accelerates in the flow direction, and the acceleration and the friction both contribute to the pressure drop. For the reverse flow, therefore, the pressure difference across the branch tube decreases as the flow travels downstream. The reverse is true for the parallel flow. Bajura and Jones [15] showed that, for single phase flow, the reverse flow yields more uniform flow distribution than the parallel flow. However, Yin et al. [16] obtained better flow distribution for the parallel flow. The magnitude of mal-distribution depends on the ratio of the header pressure drop to the branch tube pressure drop. When the ratio is large, the flow distribution becomes worse. Different header-to-tube pressure drop ratios of Bajura and Jones [15] and Yin et al. [16] appear to have yielded the opposing trend. The reason why water distribution data by Kim and Sin [12] between the reverse and the parallel flow are

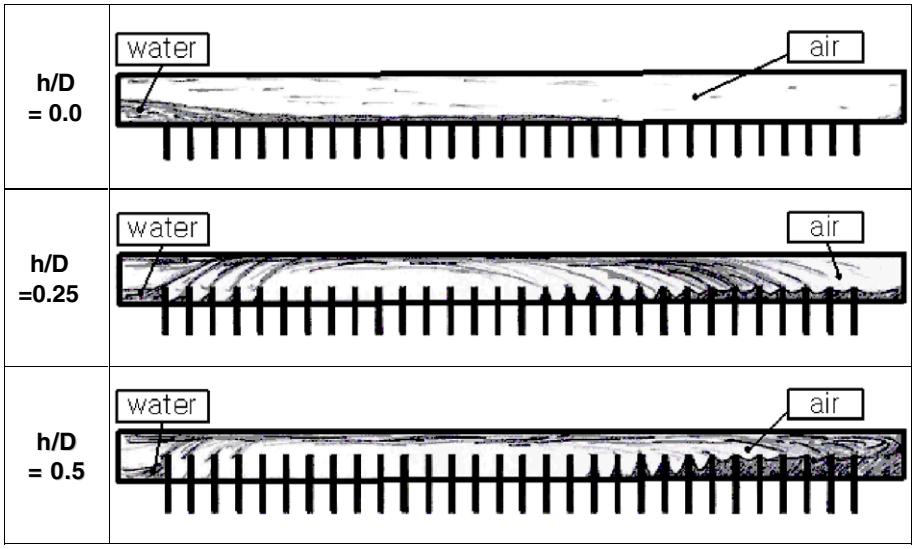

(a) Typical flow pattern in a 30 channel header with downward configuration

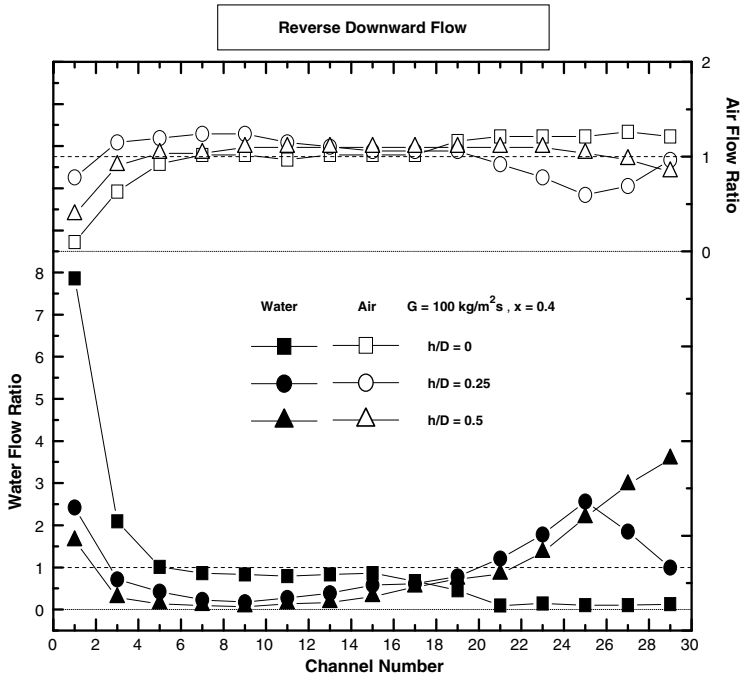

(b) Corresponding water and air distribution

Fig. 6. Typical flow pattern in a upper 30 channel header with downward flow configuration and the corresponding water and air distribution (from Kim and Sin [12]).

negligibly different is not clear. For two-phase flow, the flow distribution is affected by additional parameters such as flow regime and quality in addition to the pressure difference between headers.

3. Downward flow

3.1. Effect of tube protrusion depth

Typical flow pattern is illustrated in Fig. 5 along with the water and air distribution data for the present 10 channel. Fig. 5a shows that the flow at the inlet of the header is annular. For flush-mounted configuration ($h/D = 0$), most of the water flows into the tubes at frontal part of the header. The ordinate of the Fig. 5b is the ratio of water or air flow rate in each tube to the average values. The data taken at the header mass flux $G = 100$ kg/m^2 s and header quality $x = 0.4$ show that water flow ratio is 3.3 for the first tube, drastically decreases to 0.6 at the third tube, and then remains approximately constant afterwards. The air distribution is reverse of the water distribution. However, the variation of air distribution is much less significant

compared with that of water. In Fig. 6, 30 channel data of Kim and Sin [12] taken at the same mass flux and quality are shown. For flush-mounted configuration, the general trends of the flow distribution data are similar to those of 10 channel, although water flow ratios at frontal channels are much larger and almost no water is supplied at rear channels.

With the tube protruded into the header, the flow pattern changes significantly. As shown in the sketch of Fig. 5a, part of the incoming water impinges at the first protrusion, some of it is sucked in to the first tube, and the remaining water separates at the top. The separated water hits the rear end of the header, and supplies water from downstream. The water, which bypassed the first protrusion, along with the water from upper part of the header, impinges at the second protrusion, part of it sucked in, separates at the top and hits the rear end of the header. The process continues until no water is available for separation at the top. For the 30 channel with $h/D = 0.5$ (tube protruded to the center of the header), Fig. 6 shows that general trends of the flow pattern and the flow distribution data are similar to those of 10 channel. For $h/D = 0.25$, however, the separated water does not have enough momentum to hit the rear end of the header, and reattaches at the downstream part of the header yielding a peak of water distribution data near the reattachment point. For a 10 channel with $h/D = 0.25$, whose header length is shorter than the reattachment length, the separated water hit the rear end of the header first, yielding a peak of water distribution data at the last channel.

Kim and Sin [12] have shown that, for the 30 channel, the reattachment length increases as the tube protrusion depth, mass flux and quality increases, forcing more water to flow downstream of the header. The 10 channel flow distribution data in Fig. 5b also show that the water flow ratio at the last channel increases as the protrusion depth increases. For $h/D = 0.25$, the water flow ratio of the first channel is 2.6, decreases to 0.1 for the fifth channel, and increases to 1.7 at the last channel. For $h/D = 0.5$, the water flow ratio of the first channel is 1.9, minimum at the fifth channel, and increases to 2.4 at the last channel.

Water flow distribution data in Figs. 5 and 6 show that the differences between the maximum and the minimum water flow ratio are smaller for the 10 channel compared with those of the 30 channel (3.3, 2.4, 2.1 vs. 7.8, 2.4, 3.5 for $h/D = 0.0$, 0.25, 0.5 respectively). Comparison of the standard deviation of the water flow ratio also reveals that smaller standard deviations are obtained for the 10 channel (1.14, 0.94, 0.87 vs. 2.02, 0.83, 1.12 for $h/D = 0.0$, 0.25, 0.5, respectively). Thus, we may conclude that the water flow distribution is more uniform for the 10 channel as compared with the 30 channel. Although not shown here, similar conclusion is drawn for the air flow distribution.

The channel mass flux and quality were calculated from the measured water and air flow rates of each channel, and the results are shown in Fig. 7. The channel mass flux and quality curves are quite similar to the water and air flow

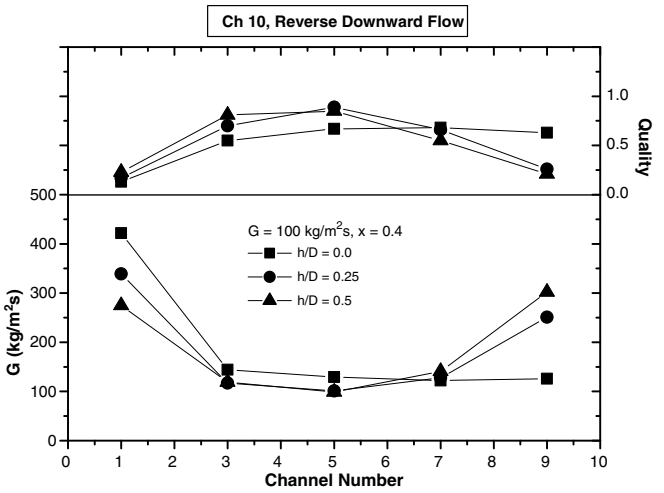

Fig. 7. Typical channel mass flux and quality with downward flow configuration.

ratio curves shown in Fig. 5b. As shown in Fig. 5b, channel water flow ratios of each channel are significantly different each other, whereas the air flow ratios are approximately the same. This may be the reason why the channel mass flux (which is the addition of the water and air mass flux) curves and the water flow ratio curves are quite similar.

In the present study, the pressure drop was measured from the inlet of the header to the channel flow measurement section (which is located 0.52 m below from the center of the header). As noted by Yin et al. [16], the measured pressure drop consists of inlet tube (64 mm long) friction, port inlet contraction loss and the tube pressure drop. Fig. 8 shows the measured pressure drop of each channel for different protrusion depths at $G = 100\ \mathrm{kg/m^2\,s}$ and $x = 0.4$. For $h/D = 0.0$, the pressure drop distribution is fairly uniform. As the protrusion depth increases, the mal-distribution of the pressure drop increases. The pressure drop of the first channel is the largest, significantly

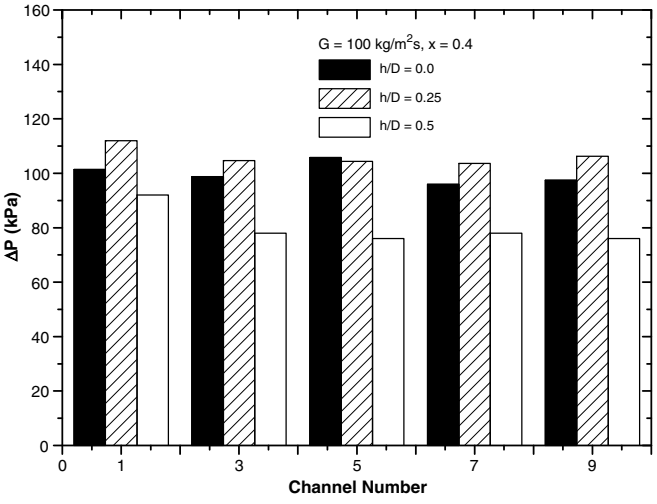

Fig. 8. Typical pressure drop from inlet of the header to flow measurement section for downward flow configuration.

decreases at the next channel (with larger decrease at larger h/D), and remains approximately the same. One interesting thing is that the pressure drops of $h/D = 0.5$ are smaller than those of $h/D = 0.0$ or $h/D = 0.25$. Improved water flow distribution at $h/D = 0.5$ (standard deviation of 0.87 compared with 1.14 at $h/D = 0.0$) may partly be responsible for the decreased pressure drop. One thing to remember is that the present pressure drop contains both the header pressure drop and the tube pressure drop.

3.2. Effect of header mass flux and quality

Fig. 9 shows the effect of header mass flux for different tube protrusion depths. For all the tube protrusion depths, more water flows through the rear part of the header as mass flux increases. For example, for $h/D = 0.5$ at $x = 0.4$ and $G = 70$ kg/m^2 s, the water flow ratio of the first tube is 1.7, decreases to 0.2 at the third tube, and then increases to 2.2 at the last tube. As the header mass flux

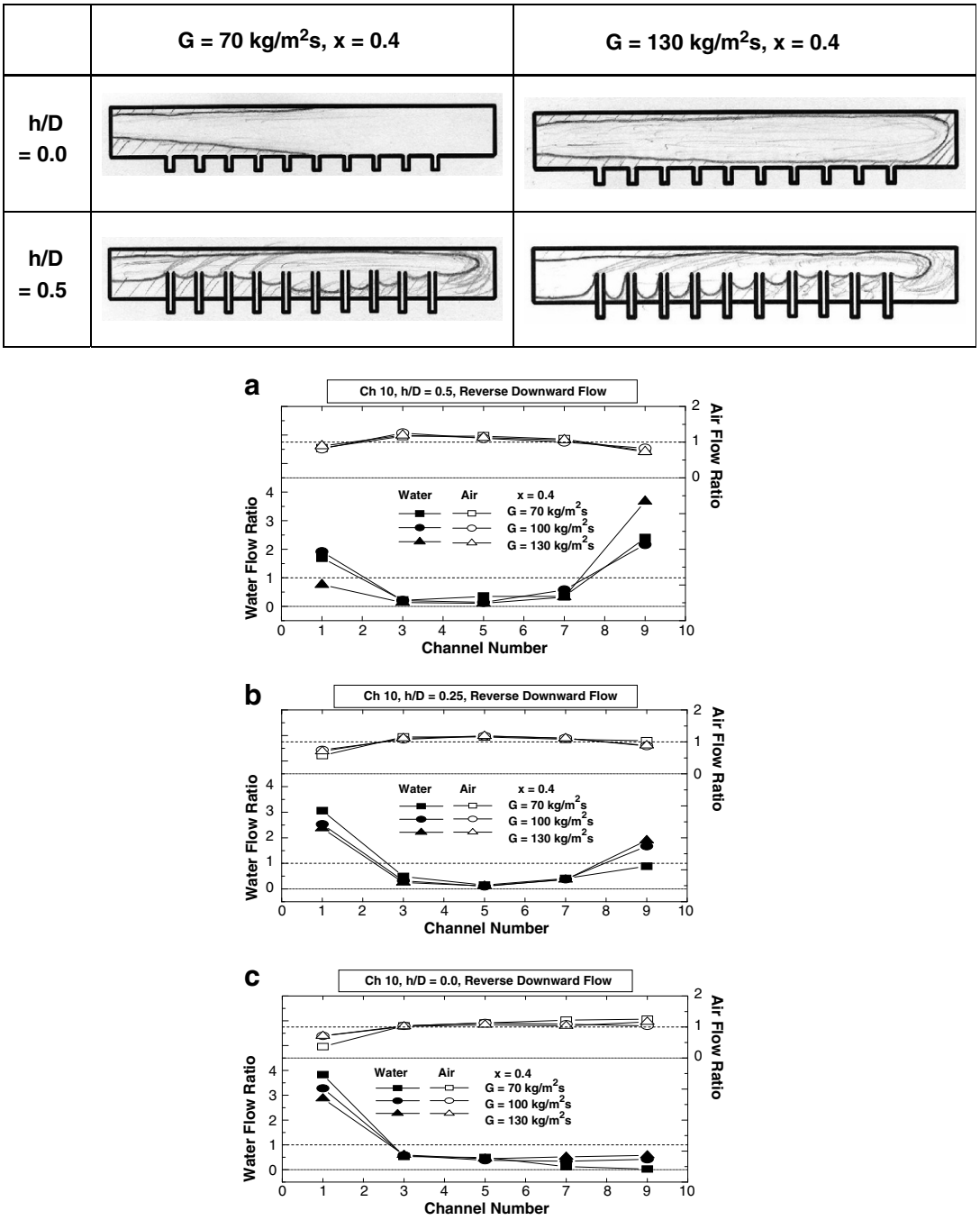

Fig. 9. Effect of header mass flux on air and water distribution in the header of downward configuration at $x = 0.4$: (a) $h/D = 0.5$, (b) $h/D = 0.25$ and (c) $h/D = 0.0$.

increases to 100 kg/m^2 s, the water flow ratio of the first tube is 1.9, and increases to 2.4 at the last tube. With further increase of mass flux to 130 kg/m^2 s, the water flow ratio of the first tube reduces to 0.8 and the maximum value of 3.8 is obtained at the last tube. The accompanying sketches confirm that, as the header mass flux increases, more water is forced to rear part of the header with thicker liquid films downstream. This trend is similar to that of the protrusion depth shown in Fig. 6. As discussed by Kim and Sin [12], the reattachment length of the separated flow from the protrusion increases as the mass flux increases due to stronger flow momentum, which forces the water to rear part of the header. The air distribution is reverse of the water distribution.

Fig. 10 shows the effect of header quality for different tube protrusion depths. These graphs are quite similar to Fig. 9. Thus, the same argument as the effect of mass flux may be provided for the effect of quality. As the quality

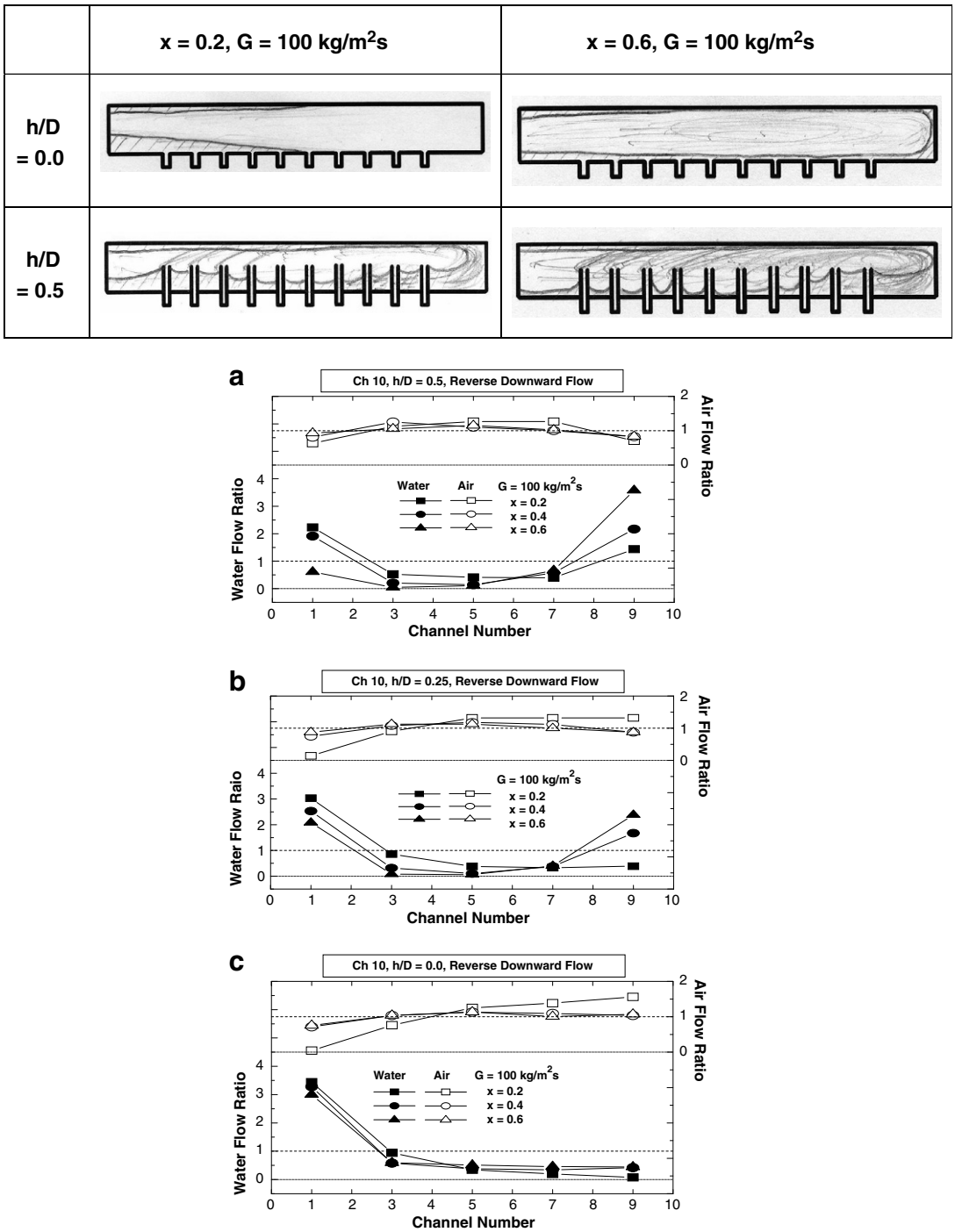

Fig. 10. Effect of header quality on air and water distribution in the header of downward configuration at $G = 100$ kg/m^2 s: (a) $h/D = 0.5$, (b) $h/D = 0.25$ and (c) $h/D = 0.0$.

increases, the reattachment length of the separated flow from the protrusions increases due to stronger flow momentum, and more water is forced to rear part of the header. Although not shown here, the 30 channel data of Kim and Sin [12] show a similar trend. More water flows to rear part of the header as the header mass flux or quality increases. Comparison of the differences between the maximum and the minimum water flow ratio along with the comparison of the standard deviations of the water flow ratio at different header mass flux and quality reveal that the flow distribution is more uniform for the 10 channel as compared with that of the 30 channel.

Bowers et al. [11] investigated the R-134a distribution in a test section composed of horizontal round header (20 mm ID) and 15 vertical flat tubes. The standard deviation of the liquid R-134a flow rate was successfully correlated by the Froude number based on cross-sectional area seen by the flow. The Froude number represents the ratio of inertial to gravitational energy of the flow, and is defined by

$$Fr = \frac{G_{\text{eff}} x}{\sqrt{\rho_v(\rho_l - \rho_v)Dg}} \quad (1)$$

In Eq. (1), G_{eff} is the effective mass flux calculated based on the flow area seen by the flow. For our geometry of 17 mm ID header with 16 mm width tube, the effective mass fluxes of $h/D = 0.25$ and 0.5 are 23% and 96% larger than that of $h/D = 0.0$ due to the protrusions. The Froude number increases as the header mass flux, quality or h/D increases. The present standard deviations of the water flow ratios and corresponding Froude numbers are listed in Table 1. Table 1 shows that, for $h/D = 0.0$, the standard deviation decreases as the Froude number increases. For $h/D = 0.5$, on the contrary, the standard deviation increases as the Froude number increases. As seen in Figs. 9 and 10, more water flows through frontal part of the header for $h/D = 0.0$ at low mass flux or quality (low Froude number). As the header mass flux or quality increases, water is forced to rear part of the header, yielding improved flow distribution. For $h/D = 0.5$ at low header mass flux or quality, however, significant amount of water flows through rear part of the header due to the separated flow from protrusions. Increasing the header mass flux or quality forces more water to rear part of the header yielding poor flow distribution. Thus, it appears that the Froude number, which successfully correlated the Bowers et al.'s R-134a data, does not correlate the present air–water data. The liquid–vapour density ratio of air–water is 845, which is approximately

Table 1
The standard deviations of the water flow ratio and corresponding Froude numbers

h/D	G/x	Fr	SD of water flow ratio	
			Downward	Upward
0.0	70/0.4	2.00	1.43	0.75
	100/0.4	2.83	1.14	0.72
	130/0.4	3.68	0.94	0.73
	100/0.2	1.42	1.26	1.31
	100/0.6	4.25	1.00	0.89
0.25	70/0.4	2.47	1.06	1.25
	100/0.4	3.49	0.94	1.13
	130/0.4	4.54	0.94	1.01
	100/0.2	1.75	1.03	1.59
	100/0.6	5.25	1.02	1.06
0.5	70/0.4	3.92	0.88	1.50
	100/0.4	5.55	0.87	1.51
	130/0.4	7.22	1.36	1.50
	100/0.2	2.78	0.73	1.64
	100/0.6	8.33	1.31	1.28

Table 2
Measured pressure drop from inlet of the header to flow measurement section

Flow direction	h/D	G/x	Pressure drop (kPa)					SD of pressure drop ratio
			Ch. 1	Ch. 3	Ch. 5	Ch. 7	Ch. 9	
Downward	0	130/0.4	169	173	175	171	170	0.012
		70/0.4	25.6	24.3	24.5	21.0	19.3	0.10
		100/0.6	148	151	154	150	174	0.061
		100/0.2	21.0	20.9	20.4	19.4	16.1	0.093
	0.5	130/0.4	171	144	145	147	141	0.073
		70/0.4	24.5	21.1	19.7	18.6	18.0	0.11
		100/0.6	155	135	143	140	135	0.52
		100/0.2	18.5	16.0	13.9	13.2	12.8	0.014
Upward	0	130/0.4	159	154	159	156	154	0.014
		70/0.4	13.1	11.4	10.9	12.2	11.9	0.093
		100/0.6	146	137	139	140	138	0.023
		100/0.2	19.0	17.9	17.7	17.6	17.1	0.035
	0.5	130/0.4	161	120	125	125	118	0.12
		70/0.4	12.2	9.1	9.7	9.2	9.8	0.11
		100/0.6	134	11.8	116	118	117	0.055
		100/0.2	16.8	15.9	15.1	14.9	14.6	0.051

23 times larger that of R-134a. In addition, the flow pattern observed by Bowers et al. [11] was stratified, whereas the present flow pattern is annular. The void fractions calculated using Zivi's [17] correlation were 0.957 and 0.993 at $x = 0.2$ and 0.6 for air–water, whereas those for R-134a were 0.736 and 0.943, respectively. Thus, the effect of protrusion on the flow distribution will be much more significant for air–water flow due to stronger interaction of the vapour flow with the protrusions.

Bajura and Jones [15] have shown that, for single phase flow, the flow distribution improves as the ratio of header pressure drop to tube pressure drop decreases. As noted previously, the present pressure drop contains both the header pressure drop and the tube pressure drop. In addition, it is not possible to extract the header pressure drop from the measured one, because channel flow rates are different one another. Typical pressure drop data are listed in Table 2, which shows that the standard deviation of the pressure drop ratio (channel pressure drop divided by the average pressure drop) improves as the header mass flux or quality increases, both for $h/D = 0.0$ and 0.5. Thus, no strong correlation is found between the standard deviation

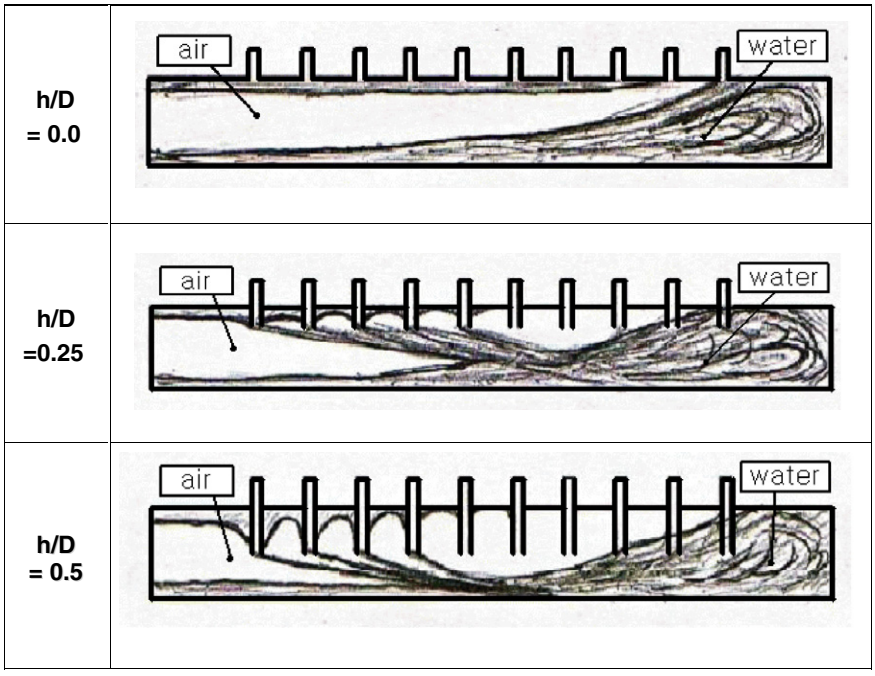

(a) Typical flow pattern in a 10 channel header with upward configuration

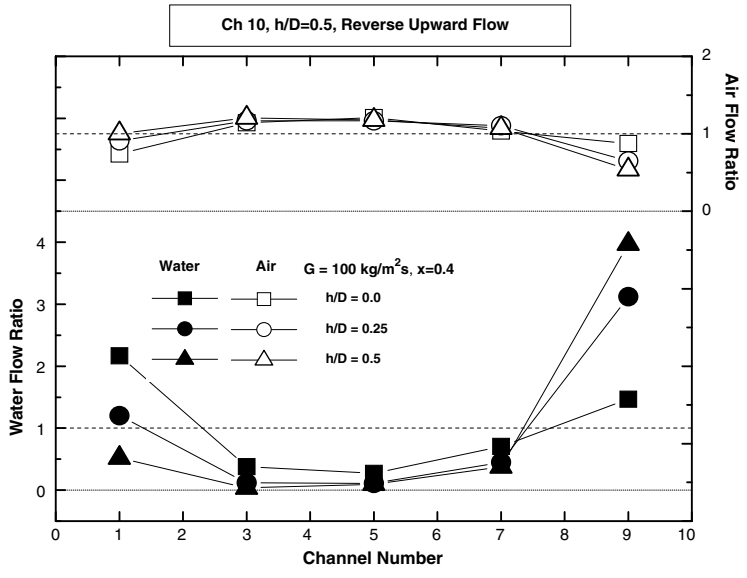

(b) Corresponding water and air distribution

Fig. 11. Typical flow pattern in a lower 10 channel header with upward flow configuration and the corresponding water and air distribution.

of water flow ratio and the standard deviation of the pressure drop ratio.

4. Upward flow

4.1. Effect of tube protrusion depth

Typical flow pattern is illustrated in Fig. 11 along with the water and air distribution data. Fig. 11a shows that the flow at the inlet of the header is annular. Different from the downward configuration, significant portion of the water flows through rear part of the header. For flush-mounted configuration ($h/D = 0$), the incoming water flowing at the upper part of the header flows into the tubes located at the frontal part of the header. The water flowing lower part of the header is forced to rear end of the header, and starts to supply the water from downstream. The data taken at $G = 100\ \mathrm{kg/m^2\,s}$, $x = 0.4$ show that water flow ratio is 2.2 for the first tube, decreases to 0.4 at the fifth tube, and then increases to 1.5 at the last tube. The air distribution is reverse of the water distribution.

With the tube protruded into the header, the flow pattern changes significantly. As shown in the sketch, the incoming water flowing at the upper part of the header impinges at the first protrusion, separates at the top, reattaches at the bottom of the header. The separated water,

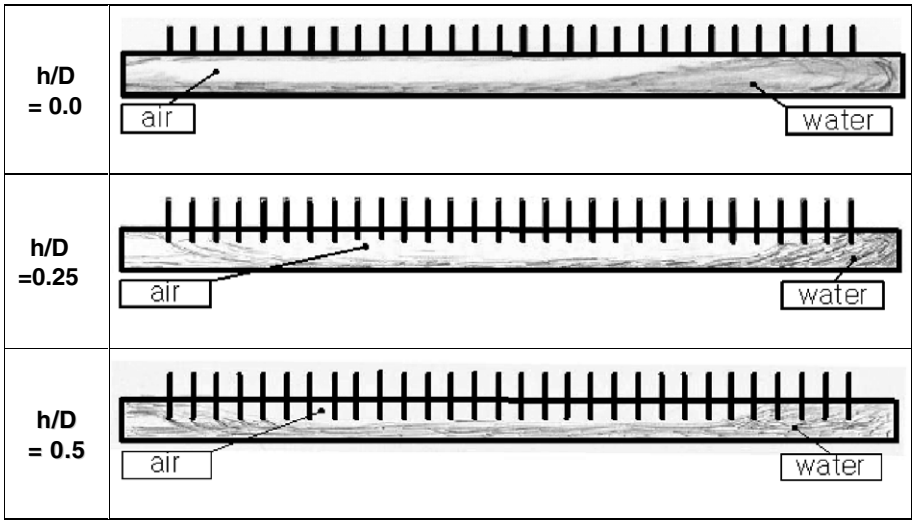

(a) Typical flow pattern in a 30 channel header with upward configuration

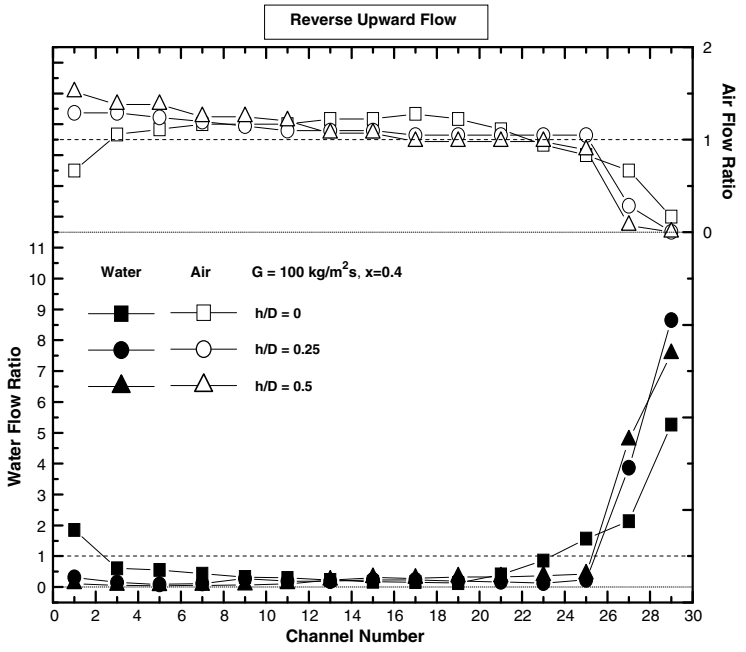

(b) Corresponding water and air distribution

Fig. 12. Typical flow pattern in a lower 30 channel header with upward flow configuration and the corresponding water and air distribution (from Kim and Sin [12]).

along with the water from lower part of the header, is forced to the rear end of the header, and is supplied from downstream. For $h/D = 0.25$, the water flow ratio is 1.2 at the first tube, decreases to 0.1 at the third tube, and then significantly increases to 2.9 at the last tube. With the tube protruded to the center of the header ($h/D = 0.5$), the water flow ratio is 0.5 at the first tube, and increases to 4.1 at the last tube. Thus, we may conclude that as the protrusion depth increases, more water is forced to rear part of the header with stronger intensity. This trend is the same as that of the downward flow. For the 30 channel, Fig. 12 shows that general trends of the flow pattern and the flow distribution data are similar to those of 10 channel. For the 30 channel, however, water flow ratios at the rear part of the header is larger as compared with those of the 10 channel. Figs. 10 and 11 also show that almost no water is supplied to the channels located at the middle of the header with much wider no-water region for the 30 channel.

Water flow distribution data in Figs. 11 and 12 show that the differences between the maximum and the minimum water flow ratio are smaller for the 10 channel compared with those of the 30 channel (1.2, 3.0, 3.9 vs. 5.2, 8.6, 7.5 for $h/D = 0.0$, 0.25, 0.5, respectively). Comparison of the standard deviation of the water flow ratio also reveal that smaller standard deviations are obtained for the 10 channel (0.72, 1.13, 1.51vs. 1.42, 2,31, 2.18 for $h/D = 0.0$, 0.25, 0.5, respectively). Thus, we may conclude that the water flow distribution is more uniform for the 10 channel as compared with the 30 channel. Similar conclusion may be drawn for the air flow distribution.

The channel mass flux and quality were calculated from the measured water and air flow rates of each channel, and the results are shown in Fig. 13. As with the downward flow, the channel mass flux and quality curves are quite similar to the water and air flow ratio curves shown in Fig. 11b. Fig. 14 shows the measured pressure drop of each channel for different protrusion depths at $G = 100$ kg/m^2 s

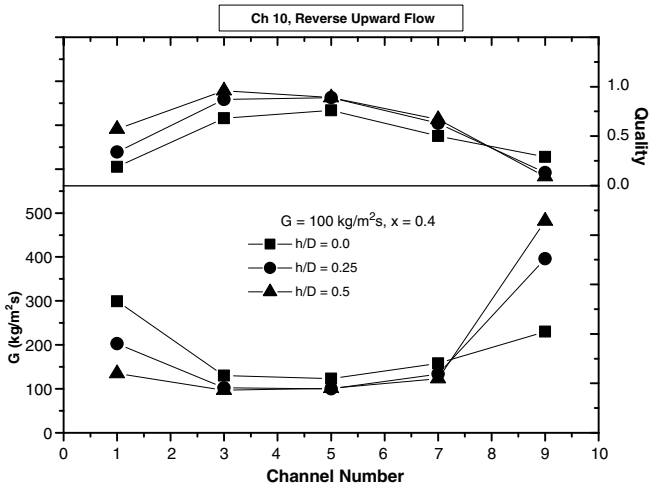

Fig. 13. Typical channel mass flux and quality with upward flow configuration.

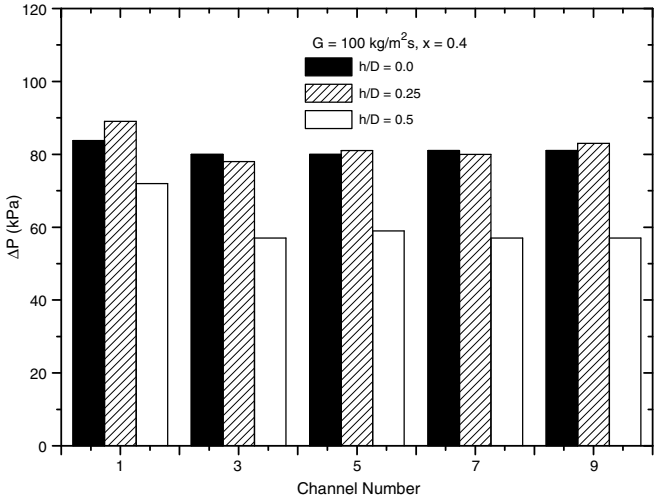

Fig. 14. Typical pressure drop from inlet of the header to flow measurement section for upward flow configuration.

and $x = 0.4$. The trends are similar to those of downward flow shown in Fig. 8. For $h/D = 0.0$, the pressure drop distribution is fairly uniform. As the protrusion depth increases, the mal-distribution of the pressure drop increases. The pressure drop of the first channel is the largest, significantly decreases at the next channel (with larger decrease at larger h/D), and remains approximately the same. The pressure drops of $h/D = 0.5$ are smaller than those of $h/D = 0.0$ or $h/D = 0.25$.

4.2. Effect of header mass flux and quality

Fig. 15 shows the effect of header mass flux for different tube protrusion depths at $x = 0.4$. The effect of quality is shown in Fig. 16. As the header mass flux or quality increases, more water flows through frontal part of the header, and less water flows through rear part of the header. The effect is getting more significant as the protrusion depth decreases. For example, for $h/D = 0.0$ at $G = 100$ kg/m^2 s and $x = 0.2$ (shown in Fig. 16c), the water flow ratio of the first tube is 0.9, decreases to 0.1 at the fifth tube, and then increases to 3.8 at the last tube. As the quality increases to 0.6, the water flow ratio of the first tube increases to 2.8, and decreases to 0.7 at the last tube. This trend is opposite to the downward flow case, where more water flows through rear part of the header as the mass flux or quality increases.

The accompanying sketches illustrate flow patterns at different header mass fluxes or qualities. For a horizontal annular flow of the present study (confirmed from the visual observation as well as from the comparison with the Baker [18] flow regime map), the water film thickness is affected by the mass flux or quality. At a high mass flux or quality, it is uniform circumferentially. At a low mass flux and quality, however, the film is thin at the top, and gets thicker towards the bottom. In addition, the average film thickness decreases as the mass flux or quality

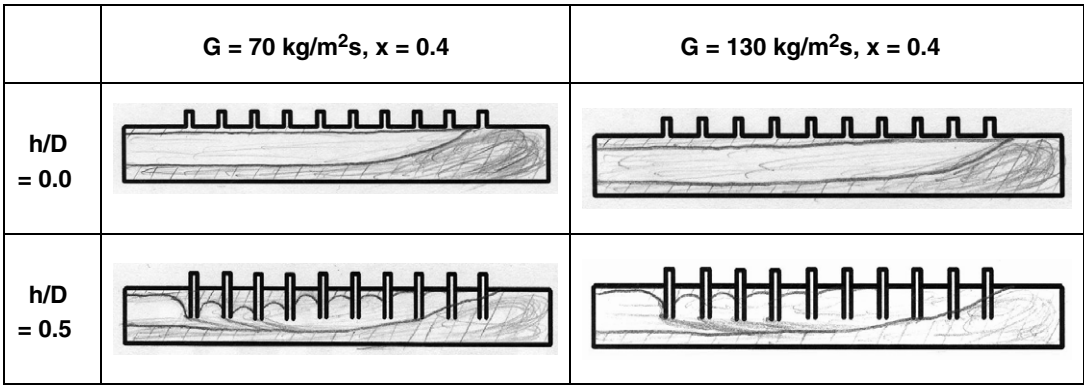

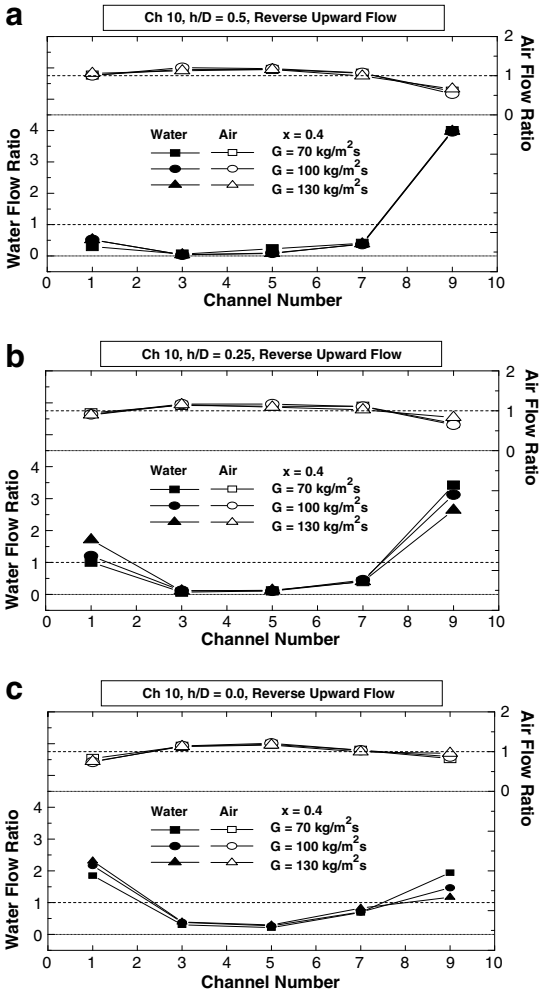

Fig. 15. Effect of header mass flux on air and water distribution in the header of upward configuration at $x = 0.4$: (a) $h/D = 0.5$, (b) $h/D = 0.25$ and (c) $h/D = 0.0$.

increases. Thickness of the water film was calculated using the void fraction model of Zivi [17] assuming a uniform peripheral film thickness. The film thickness is 0.18 mm at $x = 0.2$ and decreases to 0.03 mm at $x = 0.6$. If the water film gets thinner, more water will be sucked into the frontal channel, leaving much less for downstream channels. Thus, for the upward flow configuration, where branch tubes are located at the top of the header, more water will be supplied through frontal part of the header as the header mass flux or quality increases. If the tubes are protruded into the header, the flow separates from protrusions, and the effect film thickness on flow distribution will become weak. For a downward flow configuration, where branch channels are located at the bottom of the header, the flow distribution is affected by a rather thick water film at the bottom of the header. The thick annulus cannot be fully sucked into the frontal channels, leaving plenty of water for downstream tubes. In such a case, an increased flow momentum

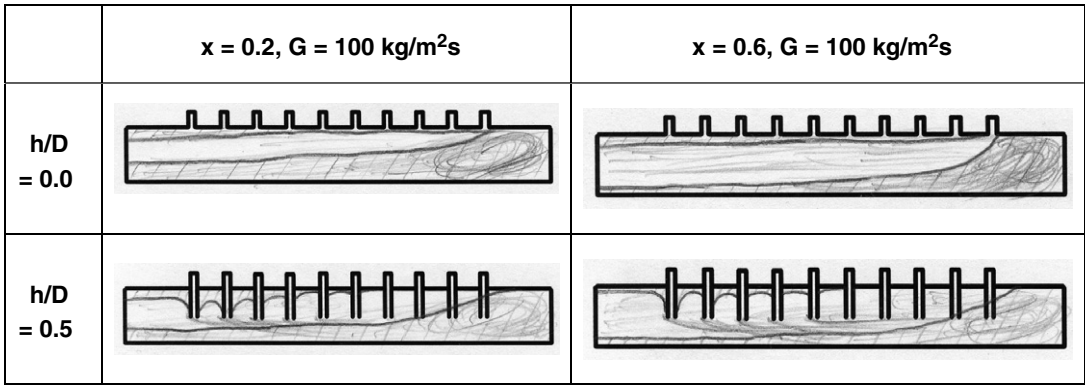

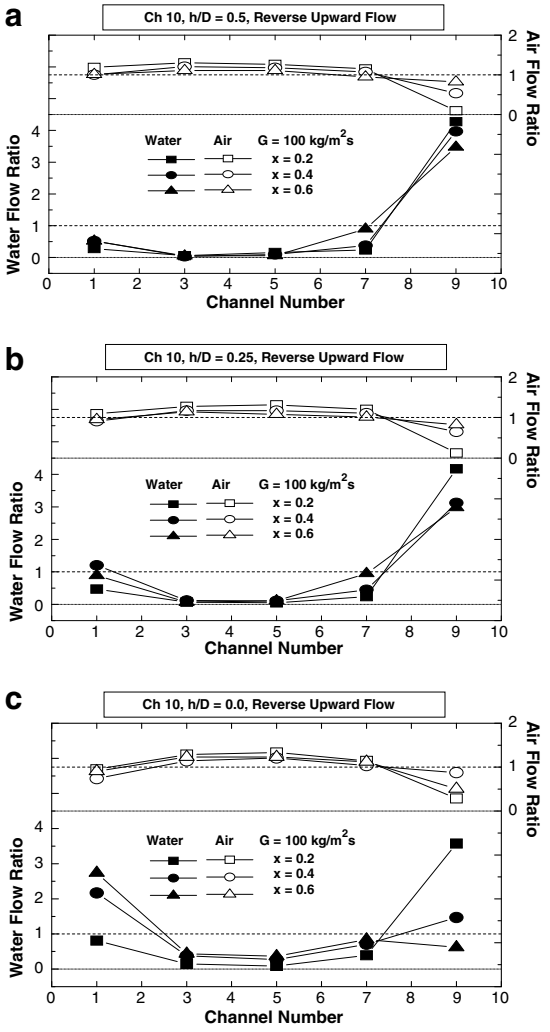

Fig. 16. Effect of header quality on air and water distribution in the header of upward configuration at $G = 100$ kg/m^2 s: (a) $h/D = 0.5$, (b) $h/D = 0.25$ and (c) $h/D = 0.0$.

induced by high header mass flux or quality will force the water to rear part of the header, supplying more water into downstream channels.

For the 30 channel configuration, Kim and Sin [12] obtained a similar flow distribution trend as that of 10 channel, although the effect of header mass flux or quality was much weaker. Comparison of the difference between the maximum and the minimum water flow ratio along with the comparison of the standard deviation of the water flow ratio reveal that the flow distribution is more uniform for the 10 channel as compared with that of the 30 channel.

The standard deviations of the water flow ratios and corresponding Froude numbers are listed in Table 1. Table 1 shows that the standard deviation is almost independent of mass flux, and decreases with the increase of quality for all the h/D ratios. The standard deviation also increases as

h/D increases. Because Froude number increases as the mass flux, quality or h/D increases, no strong correlation is found between the standard deviations and Froude numbers. Typical pressure drop data are listed in Table 2, which shows that the standard deviation of the pressure drop ratio improves as the mass flux or quality increases, especially for $h/D = 0.0$. Thus, no strong correlation is found between the standard deviation of the pressure drop ratio and the standard deviation of the water flow ratio.

5. Conclusions

In this study, the air and water flow distribution are experimentally studied for a parallel flow heat exchanger composed of round headers and 10 flat tubes. The effects of tube protrusion depth as well as header mass flux, and quality are investigated, and the results are compared with the previous 30 channel data. The flow at the header inlet is annular.

(1) For the downward flow, the water flow distribution is significantly affected by the tube protrusion depth. For flush-mounted configuration, significant portion of the water flows through frontal part of the header. As the protrusion depth increases, more water is forced to the rear part of the header.
(2) For the downward flow, the effect of header mass flux or quality is qualitatively the same as that of the protrusion depth. Increase of the header mass flux or quality forces the water to rear part of the header.
(3) For the upward flow, significant portion of the water flows through rear part of the header. The effect of the protrusion depth is the same as that of the downward flow. As the protrusion depth increases, more water is forced to the rear part of the header.
(4) For the upward flow, the effect of header mass flux or quality is opposite to the downward flow case. As the header mass flux or quality increases, more water flows through the frontal part of the header.
(5) As the protrusion depth increases, the mal-distribution of the pressure drop (which includes both header and channel pressure drop) increases. The pressure drop of the first channel is the largest, significantly decreases at the next channel (with larger decrease at larger h/D), and remains approximately the same. The pressure drops of $h/D = 0.5$ are smaller than those of $h/D = 0.0$ or $h/D = 0.25$.
(6) The general flow distribution trend of the 10 channel is approximately the same that of the 30 channel, although the effects of tube protrusion depth, header mass flux and quality on flow distribution are much stronger. Comparison of the difference between the maximum and the minimum water flow, and the comparison of the standard deviation of the water flow ratio reveal that the flow distribution is more uniform for the 10 channel as compared with the 30 channel.

Acknowledgement

This work was supported by the Korea Research Foundation Grant funded by the Korean Government (R05-2003-000-10170).

References

[1] T. Kulkarni, C.W. Bullard, K. Cho, Header design tradeoffs in microchannel evaporators, Appl. Therm. Eng. 24 (2004) 759–776.
[2] R.L. Webb, K. Chung, Two-phase flow distribution in tubes of parallel flow heat exchangers, Heat Transfer Eng. 26 (2004) 3–18.
[3] P. Hrnjak, Flow distribution issues in parallel flow heat exchangers, ASHRAE Annual Meeting, AN-04-1-2, 2004.
[4] S.Y. Lee, Flow distribution behaviour in condensers and evaporators, in: Proceedings of the 13th International Heat Transfer Conference, KN-08, Sydney, Australia, August, 2006.
[5] M. Watanabe, M. Katsuda, K. Nagata, Two-phase flow distribution in multi-pass tube modeling serpentine type evaporator, ASME/JSME Therm. Eng. Conf. 2 (1995) 35–42.
[6] D.M. Tompkins, T. Yoo, P. Hrnjak, T. Newell, K. Cho, Flow distribution and pressure drop in micro channel manifolds, in: Proceedings of the 9th International Refrigeration and Air Conditioning Conference at Purdue, R6-4, 2002.
[7] S. Vist, J. Pettersen, Two-phase flow distribution in compact heat exchanger manifolds, Exp. Therm. Fluid Sci. 28 (2004) 209–215.
[8] J.K. Lee, S.Y. Lee, Distribution of two-phase annular flow at header-channel junctions, Exp. Therm. Fluid Sci. 28 (2004) 217–222.
[9] H. Cho, K. Cho, Y. Kim, Mass flow rate distribution and phase separation of R-22 in multi-microchannel tubes under adiabatic condition, in: Proceedings of the 1st International Conference Microchannels and Minichannels, 2003, pp. 527–533.
[10] S. Koyama, A.T. Wijayanta, K. Kuwahara, S. Ikuda, Developing two-phase flow distribution in horizontal headers with downward micro-channel branches, in: Proceedings of the 11th International Refrigeration and Air Conditioning Conference at Purdue R142, July, 2006.
[11] C.D. Bowers, P.S. Hrnjak, T.A. Newell, Two-phase refrigerant distribution in a micro-channel manifold, in: Proceedings of the 11th International Refrigeration and Air Conditioning Conference at Purdue R161, July, 2006.
[12] N.H. Kim, T.R. Sin, Two-phase flow distribution of air–water annular flow in a parallel flow heat exchanger, Int. J. Multiphase Flow 32 (2006) 1340–1353.
[13] X. Rong, M. Kawaji, J.G. Burgers, Two-phase header flow distribution in a stacked plate heat exchanger, FED-Gas Liquid Flows 225 (1995) 115–122.
[14] P. Bernoux, P. Mercier, M. Lebouche, Two-phase flow distribution in a compact heat exchanger, in: Proceedings of the 3rd International Conference Compact Heat Exchangers, 2001, pp. 347–352.
[15] R.A. Bajura, E.H. Jones, Flow distribution manifolds, J. Fluids Eng. 98 (1976) 654–666.
[16] J.M. Yin, C.W. Bullard, P.S. Hrnjak, Single-phase pressure drop measurements in a microchannel heat exchanger, Heat Transfer Eng. 23 (2002) 3–12.
[17] S.M. Zivi, Estimation of steady state steam void fraction by means of principle of minimum entropy production, Trans. ASME, Series C 86 (1964) 237–252.
[18] O. Baker, Design of pipe lines for simultaneous flow of oil and gas, Oil Gas J. 26 (July) (1954).